Extraction of Coseismic Displacement in the November 22, 2014 Nagano, Japan Earthquake from ALOS-2 Images

Wen Liu, Luis Moya, and Fumio Yamazaki
Graduate School of Engineering, Chiba University
Chiba University
1-33 Yayoi-cho, Inage-ku, Chiba, Japan
wen.liu@chiba-u.jp; lmoyah@uni.pe; fumio.yamazaki@faculty.chiba-u.jp

***Abstract*— An Mw6.2 earthquake hit northern Nagano prefecture, Japan on November 22, 2014, with 46 people injured and a lot of damage to houses. Due to the fault movement, about 1-m displacement was observed by field surveys after the earthquake. Interferomatic SAR (InSAR) analysis has been confirmed as an effective tool to detect displacements in the centimeter level. In this study, the pre- and post-event ALOS-2 PALSAR-2 data were used to grasp the displacements around the Kamishiro Fault by the differential InSAR analysis. The slant range movements were obtained according to the phase differences. Then a fault model was built by introducing the parameters published by the Global Centroid-Moment-Tensor Catalog. A three-dimensional displacement was simulated using the fault model and it was compared with the observation result by a GPS ground station and at a strong-motion station.**

***Index Terms*—fault model, displacement, GEONET, strong-motion station, inversion.**

I. Introduction

An Mw6.2 earthquake jolted northern Nagano prefecture, Japan at 22:08 (local time) on November 22, 2014. The epicenter was located at 36.64º N, 137.89º E with 9.0 km depth. It was an intraplate earthquake with reverse faulting, and caused numerous fault scarps. Due to the strong shaking, about 1,500 buildings were damaged and 46 people were injured. According to field surveys after the earthquake, about 1-m displacement was observed around the fault trace. This earthquake was caused by the movement of the Kamishiro Fault. This fault is a northern part of the Itoigawa-Shizuoka Tectonic Line, which is a major fault in Honshu island of Japan. Although there are seven ground stations of the GPS observation network system (GEONET), installed by the Geospatial Information Authority of Japan (GSI), near the main Kamishiro Fault, only the station "Hakuba" reported the displacements larger than 30 cm in the horizontal and 0.14 cm in the vertical (subsidence) directions. It was difficult to grasp the detailed movements only from the GPS records.

Remote sensing technology using satellite images is an effective tool to grasp a large-scale coseismic deformation. Two kinds of methods are normally used for the displacement measurement. One is cross-correlation (pixel-offset) method, which can measure the relative two-dimensional displacement between two images in a pixel to sub-pixel scale [1-2]. The other one is an interferometric analysis of synthetic aperture radar (InSAR), which can obtain the displacements to the line-of-sight direction. Many researches have conducted the detection of daily and coseismic displacements [3-4]. InSAR method can measure displacements at a centimeter level, despite its meter-level spatial resolution. However, more than two pairs of imagery data are necessary to detect the three-dimensional (3D) displacements for the both methods.

There was no effective tool to monitor deformation for forest areas in the recent period, since the satellite ALOS stopped the observation in April 2011 after the Tohoku earthquake. The successor, ALOS-2, with a more powerful L-band sensor was finally launched in May 2014 and began operation. The revisit time of ALOS-2 was shorten to 14 days, and the dual receiving antenna system improves the resolution of the PALSAR-2 sensor up to 1-3 m. The 2014 Nagano earthquake was the first big earthquake event with the significant ground deformation under PALSAR-2 observation.

In this study, the displacements due to the earthquake around the Kamishiro Fault are detected using the pre- and post-event ALOS-2 PALSAR-2 data by the differential interferometric SAR (DInSAR) analysis. The obtained phase is unwrapped and transformed into the actual movements observed in the sensor range direction. In addition, a fault model is built according to the parameters obtained from the Global Centroid-Moment-Tensor (CMT) Catalog [5]. The 3D displacements simulated from the fault model are compared with the observation data by a GPS ground station and at a strong-motion station.

II. Study Area and Imagery Data

The study area was focused on the Kamishiro Fault in Nagano prefecture, Japan, as shown in Fig. 1(a). According to the Instrumental Seismic Intensity image cited from QuiQauke, strong shaking occurred in a narrow area around the fault [6]. The pre-event PALSAR-2 image was taken on October 2, whereas the post-event one was taken on November 27, 2014.

978-1-4673-7297-8/15/$31.00 ©2015 IEEE

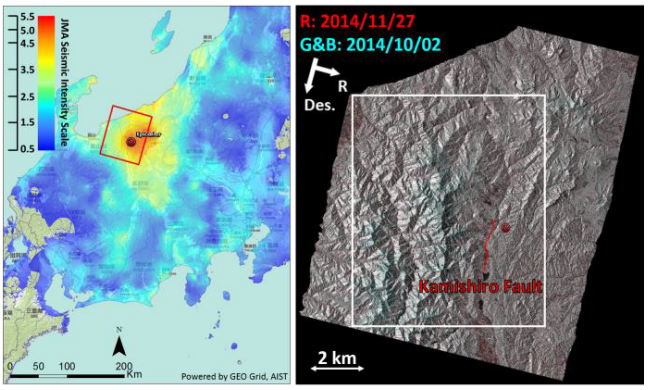

(a) (b)

Fig.1. Instrumental intensity in JMA seismic scale published by QuiQuake [6], overlapping on the study area (a); the color composite of the geo-coded pre- and post-event ALOS-2 PALSAR-2 intensity images, and the location of the Kamishiro Fault (b).

The two data were taken in the descending path by the left looking. The incident angle at the center was 36.18°. The acquisition mode was the Strip Map (SM), with 3-m resolution in both the azimuth and range directions. The PALSAR-2 data were provided as Single Look Complex (SLC) products at the processing level 1.1.

The processing steps were carried out using the software *ENVI/SARscape*. A multi-looking process was applied to both the azimuth and range direction as 2×2, and then the spacing size was changed to 4 m in the azimuth direction and 2.8 m in the range direction, respectively. A 30-m ASTER Global Digital Elevation Model (GDEM) was introduced to project the data to a WGS84 reference ellipsoid with a resampled square pixel size of 5 m. GDEM is a DEM product developed and published by the Ministry of Economy, Trade, and Industry (METI) of Japan and the United States National Aeronautics and Space Administration (NASA), which is generated from the stereo-pair of ASTER images [7]. A color composite image of the pre- and post-event intensity images was generated and shown in Fig. 1(b). Owing to the high resolution, the backscatter changes in agriculture fields, the water level in rivers and several large buildings could be confirmed. However, the surface rupture could not be observed from the SAR intensity images.

III. Differential Interferometric SAR Analysis

A DInSAR analysis was applied to the complex products of the slant-range PALSAR-2 data using the *SARscape* software to detect the crustal movement. Firstly, the pre- and post-event data were co-registered in a sub-pixel level. An initial InSAR result within the white frame of Fig. 1(b) was obtained using the phase information of the two images. Since the normal baseline between the pre- and post-event data was only 7 m, the height for one fringe from $-\pi$ to π represents 7832.5 m. Thus, the influence of the elevation was small. Then the GDEM was introduced to remove elevation effects from the initial result. Orbital fringes and noises were reduced by a Goldstein filter [8]. Finally, the enlarged geocoded coherence image was obtained and shown in Fig. 2(a) by a rainbow color.

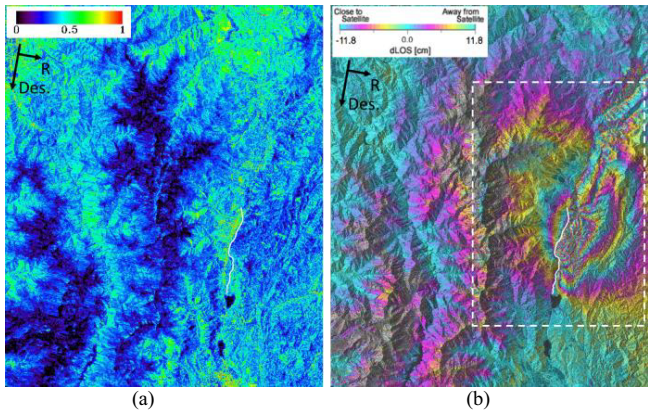

(a) (b)

Fig.2. Geocoded coherence image (a) and the composite image of the re-flattened phase and intensity (b).

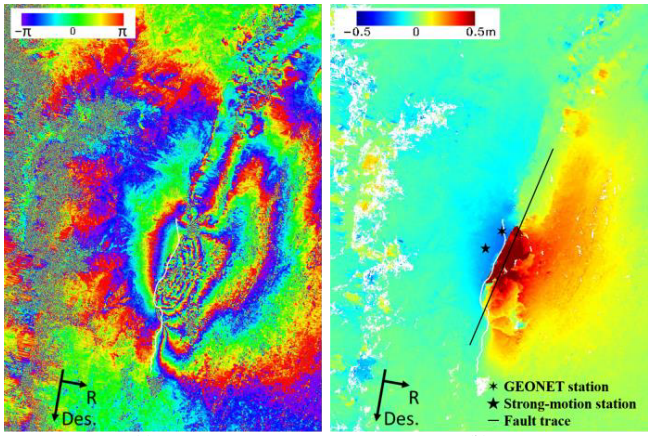

(a) (b)

Fig.3. A close-up of the re-flattened phase (a); the unwrapped displacements in the line-of-sight direction, where the positive value represents the movement toward to the sensor direction (b).

Despite of the short baseline distance, the peaks of mountains show low coherence, which could be accounted for snowfall.

The fringes caused by the coseismic deformation between $-\pi$ and π were obtained from the areas with a higher coherence than 0.25. To remove the phase offset, 9 ground control points (GCPs) were selected manually in the stable area with high coherence and far away from the fault. The composite image of the re-flattened fringes and intensity is shown in Fig. 2(b), and a close-up of the phase in the white dotted frame is shown in Fig. 3(a). Comparing with the smooth deformation in the west side, 8 fringes in the maximum could be counted in the east side of the fault, which represents about 1-m displacement. From the figure, significant displacements around the Kamishiro Fault could be confirmed. The east side of the fault moved close to the sensor direction whereas the west side moved to the away direction.

The fringes were unwrapped by the Minimum Cost Flow method [9]. This method considers a square grid over the image pixels, and is enable to overcome the presence of large areas with low coherence. The dense fringes near the fault could not be unwrapped successfully due to the low coherence. A manual edit was made to revise the unwrapped result, and the final displacement to the slant-range direction is shown in

Fig. 3(b). The positive values in the red color represent the displacements toward to the sensor direction. The largest displacements were estimated as 0.73 m close to the sensor direction in the east and 0.30 m away in the west. A GEONET ground station "Hakuba" is located at the west side of the fault, as shown in Fig. 3(b). Comparing with the record on October 2, 2014 when the pre-event record was acquired, 0.27-m displacement to the east, 0.15-m to the south and 0.14-m subsidence were observed after the earthquake. According to the incident angle, the location of the Hakuba station moved 0.40-m away from the sensor direction, whereas 0.26-m displacement was estimated from the DInSAR analysis. Although the unwrapped result has been refined by the GCPs, there still exists off-set.

IV. Estimation of 3D Displacement from the Fault Model

3D surface displacements can be obtained by using more than two SAR image pairs that are captured from ascending and descending orbits [10-11]. However, there is no suitable data for many cases. For detecting the deformation caused by the earthquake, the slip distribution also can be estimated from the fault model. In this study, a fault model was built according to the displacements obtained by the DInSAR analysis. Then the 3D displacements were simulated using the fault model.

First, the displacements to the line-of-sight direction were subsampled as vector data. Two different resolutions of subsampling were used. The resolution for the area with the significant displacements and close to the fault trace was set as 500 m whereas the surrounding area was 2000 m. 1149 points were totally resampled from the target area. The transformed vector data were shown in Fig. 4(a) with a 3D view. Uplift points represent the movements toward to the sensor direction.

Then a nonlinear inversion was carried out to find the best-fit single fault by means of an elastic dislocation [12]. Since the source model was unknown, the parameters published in the Global CMT catalog for the mainshock were adopted as the initial values. From the observation data of several strong-motion seismometers, a CMT solution was calculated with the centroid location at 36.74° N, 137.93° W and 12.0 km depth. Two planes were obtained with 13° and 249° strike angles. The plane with 13° strike, 51° dip and 47° rake was adopted according to the InSAR analysis result. After several round calculations, a fault model with 23° strike, 60° dip and 50° rake was determined as the most-suitable single fault plane. The fault plane was about 15 km in length and 13 km in width, as shown in Fig. 4(a). The surface trace of the fault plane is also shown in Fig. 3(b), paralleling to the known Kamishiro Fault. The moment magnitude for the estimated fault model is 6.45, larger than the 6.25 CMT-solution. Comparing with the observed displacements from the SAR data, the overall root mean square (RMS) error for the simulated slip distribution in the line-of-sight direction was 7 cm.

With the nonlinear inversion, an average source model was inferred. To retrieve a more realistic slip distribution, a linear inversion was also carried out. The single fault estimated by the nonlinear inversion was extended to 22 km in length and 16

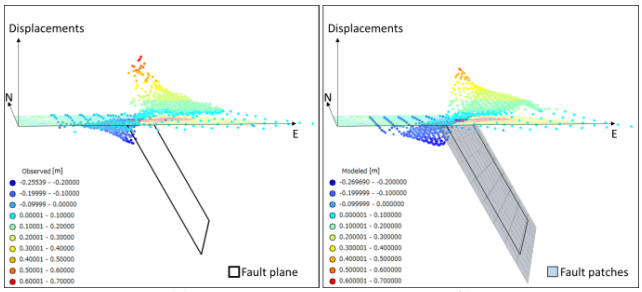

(a) (b)

Fig.4. 3D view for the unwrapped displacements in the line-of-sight direction, which have been subsampled as vector data, and the fault plane estimated by the non-linear inversion (a); modeled displacements after the linear inversion by extending and subdivided the fault plane into 11×8 patches (b).

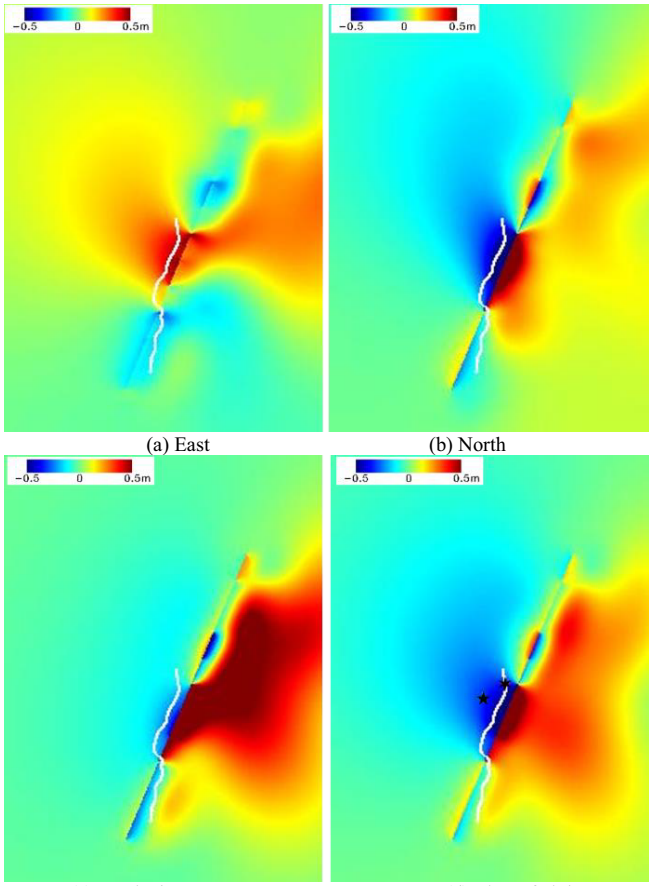

(a) East (b) North

(c) Vertical (d) Line-of-sight

Fig.5. Simulated slip distribution from the final fault model after the linear inversion to the east (a), north (b), vertical (c), and line-of-sight (d) directions, respectively.

km in width, covering the whole slipped area. Then the fault plane was divided into 2-km patches, as shown in Fig. 4(b). After the nonlinear inversion, an average slip was obtained as 0.92 cm. In the linear inversion, the unique slip for each patch was calculated again according to the DInSAR results. The final modeled displacements in the line-of-sight direction are shown in Fig. 4(b). Comparing with the observed results shown in Fig. 4(a), the same tends of deformation in the east and west sides of the main fault could be confirmed. Since the slips were

calculated in a small local area (2-km patch), the modeled results showed different values at several locations. The value range of the modeled results was from -0.27 m to 0.53 m in the line-of-sight direction, similar to the one of the observed results, which was from -0.26 m to 0.71 m. The simulated displacement as the Hakuba GEONET station was 0.37-cm away whereas the observed GPS record was 0.40-cm away.

Excepting the GPS observation and remote sensing technology, the permanent displacements due to the earthquake can also be measured from strong-motion records. After the 1995 Hyogoken-Nanbu (Kobe) earthquake, the National Research Institute for Earth Science and Disaster Prevention (NIED) constructed two strong-motions networks, which are named Kyoshin Network (K-NET) and Kiban-kyoshin Network (KiK-net). There are more than 1,700 strong-motion stations installed over the entire Japan. In the target area of this study, the K-NET "Hakuba" station was established near the Kamishiro Fault, as shown in Fig. 3(b). After the double integration of acceleration records and a baseline correction, the permanent displacement was obtained as 0.22 m to the east, 0.13 m to the south and 0.09 m subsided. Since the K-NET station locates in the same side with the GEONET station that is about 2-km away, the observed displacements are similar. The displacement at the K-NET station was 0.30-cm away in the line-of-sight direction whereas the simulated slip was 0.33-cm away. The overall RMS error was improved to 6 cm after the linear inversion.

After the determination of the fault model, the displacements to the east, north and vertical directions were simulated by a rectangular dislocation in a homogeneous and elastic half-space. The simulated 3D displacements in the same area with Fig. 3(b) are shown in Fig. 5(a-c). Since the fault plane was extended to 22 km along the strike direction, the displacements could be identified in a long area. According to the simulation, the east-side of the fault moved to the northeast and uplifted whereas the west side of the fault moved to the southeast and subsided. Comparing with the observed data at the GEONET and K-NET stations, the same trends in the three directions could be confirmed. However, it is difficult to confirm the movements in the east-side of the fault due to the lack of observed data. At the GEONET station, the simulated displacement was 0.36 cm to the east, 0.43 cm to the south and 0.14 m subsidence. The errors in the east and vertical directions were smaller than 10 cm, however that in the north direction is 27 cm. At the K-NET station, the simulated displacement was 0.31 cm to the east, 0.30 cm to the south and 0.14 m subsidence, which was similar with that from the strong-motion records. More than 1-m vertical displacement was obtained by the simulation near the fault trace, especially in the north part of the fault, which was match with field survey reports. The displacements in the line-of-sight direction were also calculated by the 3D slips as depicted in Fig. 5(d), which shows the similar distribution as Fig. 3(b).

V. Conclusions

In this study, the displacements caused by the 2014 Nagano, Japan earthquake were detected from the pre- and post-event ALOS-2 PALSAR-2 data. The displacements in the line-of-sight direction were obtained by a DInSAR analysis first. Then a fault model was built by fitting the slip distribution with the DInSAR results. After nonlinear and linear inversions, the fault plane with 1-km patches was determined. The 3D displacements were estimated by the simulation with the fault model. Comparing with the observation records at a GPS ground station and at a strong-motion station, reasonable displacements in the three-directions could be obtained by the proposed method.

Acknowledgment

The ALOS-2 PALSAR-2 data used in this study are owned by Japan Aerospace Exploration Agency (JAXA), and are provided through the JAXA's PI workshop.

References

[1] M. Tobita, H. Suito, T. Imakiire, M. Kato, S. Fujiwara, and M. Murakami, "Outline of vertical displacement of the 2004 and 2005 Sumatra earthquakes revealed by satellite radar imagery," Earth Planets Space, vol. 58, pp. e1–e4, 2006.

[2] S. Leprince, S. Barbot, F. Ayoub, and J.-P. Avouac, "Automatic and precise orthorectification, coregistration, and subpixel correlation of satellite images, application to ground deformation measurements," IEEE T. Geosci. Remote., vol.45, pp. 1529–1558, 2007.

[3] S. Stramondo, F.R. Cinti, M. Dragoni, S. Salvi, and S. Santini, "The August 17, 1999 Izmit, Turkey, earthquake: Slip distribution from dislocation modeling of DInSAR and surface offset," Ann. Geophys.-Italy, vol. 45, pp. 527–536, 2002.

[4] C. Wicks, C. Weaver, P. Bodin, and B. Sherrod, "InSAR evidence for an active shallow trust fault beneath the city of Spokane Washington, USA," J. Geophys. Res.–Sol. Ea., vol. 118, pp. 1268–1276, 2013.

[5] Global Centroid-Moment-Tensor (CMT) Project (2010): http://www.globalcmt.org/

[6] QuiQuake: https://gbank.gsj.jp/QuiQuake/index.en.html

[7] T. Tachikawa, M. Hato, M. Kaku, and A. Iwasaki, "The characteristics of ASTER GDEM version 2," IGARSS, pp. 3657-3660, 2011.

[8] R.M. Goldstein, and C.L. Werner, "Radar Interferogram Filtering for Geophysical Applications," Geophysical Research Letter, vol.25, no.21, pp.4035-4038, 1998.

[9] M. Costantini, "A novel phase unwrapping method based on network programming," IEEE T. Geosci. Remote., vol.36, no.3, pp.813-821, 1998.

[10] L. Zhang, J.C. Wu, L.L. Ge, X.L. Ding, and Y.L. Chen, "Determining fault slip distribution of the Chi-Chi Taiwan earthquake with GPS and InSAR data using triangular dislocation elements," J. Geodyn., vol. 45, pp. 163–168, 2007.

[11] J. Beavan, E. Fielding, M. Motagh, S. Samasonov, and N. Donnelly, "Fault location and slip distribution of the 22 February 2011 Mw 6.2 Christchurch, New Zealand, Earthquake from geodetic data," Seismol. Res. Lett., vol. 82, pp. 789–799, 2011.

[12] Y. Okada, "Surface deformation due to shear and tensile faults in a half-space," Bulletin of the Seismological Society of America, Vol.75, pp.1135–1154, 1985.